ADVANCED FUNCTIONAL MATERIALS
www.afm-journal.de

# Biomimetic Spider Silk by Crosslinking and Functionalization with Multiarm Polyethylene Glycol

*Viktors Romaņuks, Jēkabs Fridmanis, Benjamin Schmuck, Anna Līna Bula, Alons Lends, Kristine Senkane, Gundars Leitis, Sergejs Gaidukovs, Krisjanis Smits, Anna Rising, Gints Smits, and Kristaps Jaudzems**

**Spider silk is renowned for its exceptional mechanical properties, surpassing those of other natural and many synthetic fibers. Yet, replicating its remarkable properties through synthetic production remains a challenge. The variability in the mechanical properties of synthetic spider silks lacking protective coatings, exacerbated by factors such as spinning conditions and humidity levels, poses an additional challenge, impacting their application potential. Bioconjugation offers a versatile synthetic method to modify protein structures, enhancing their pharmacokinetics, solubility, stability, and immune response. In particular, polyethylene glycol (PEG)-ylation has emerged as a successful strategy with numerous marketed PEG–protein conjugates. This study introduces synthetic spider silk—multiarm PEG bioconjugates, facilitating spidroin crosslinking, and chemical functionalization while retaining a biomimetic spinning approach. Two different examples demonstrate the potential of this approach to improve the fiber's tensile strength and extensibility, respectively, both leading to an increased toughness modulus. Furthermore, the approach could allow the tuning of fiber mechanical properties without developing a new mini-spidroin construct and fiber coating with lipids attached to multiarm PEG, potentially mitigating the impact of environmental conditions on synthetic spider silk fibers.**

## 1. Introduction

Spider silk is a remarkable biomaterial with extraordinary mechanical properties that surpass those of most natural and synthetic fibers.[1] It offers a unique combination of high tensile strength, high elasticity, high modulus,[2] and biocompatibility.[3] These properties render it a promising material for applications in tissue engineering and regenerative medicine, such as scaffolds for growing new tissues and artificial organs.[4,5] Ongoing research in biomedicine and materials science continues to explore the potential applications of this remarkable material, although the production of synthetic spider silk still faces challenges that need to be overcome.[6]

Spider silk is a highly ordered protein fiber, and its organization at the molecular and secondary structure levels is determined by the spider silk protein (spidroin) amino acid sequence and their

V. Romaņuks, J. Fridmanis, A. L. Bula, A. Lends, K. Senkane, G. Leitis, G. Smits, K. Jaudzems
Latvian Institute of Organic Synthesis
Aizkraukles 21, Riga LV-1006, Latvia
E-mail: kristaps.jaudzems@osi.lv

B. Schmuck, A. Rising
Department of Medicine Huddinge
Karolinska Institute
Neo, Huddinge 14183, Sweden

B. Schmuck, A. Rising
Department of Animal Biosciences
Swedish University of Agricultural Sciences
Box 7023, Uppsala 75007, Sweden

S. Gaidukovs
Institute of Chemistry and Chemical Technology
Faculty of Natural Sciences and Technology
Riga Technical University
P. Valdena Str. 3, Riga LV-1048, Latvia

K. Smits
Baltic Biomaterials Centre of Excellence
Headquarters at Riga Technical University
P. Valdena Str. 3, Riga LV-1048, Latvia

K. Smits
Institute of Biomaterials and Bioengineering
Faculty of Natural Sciences and Technology
Riga Technical University
P. Valdena Str. 3, Riga LV-1048, Latvia

K. Jaudzems
Faculty of Medicine and Life Sciences
University of Latvia
Jelgavas 1, Riga LV-1004, Latvia

The ORCID identification number(s) for the author(s) of this article can be found under https://doi.org/10.1002/adfm.202409487



**DOI: 10.1002/adfm.202409487**

structural transformations during the assembly process.[7] The spidroins consist of three structural subunits, including two nonrepetitive N- and C-terminal domains (NT and CT), which regulate the silk formation process,[8,9] and a central highly repetitive region (Rep) that contributes most to the mechanical properties of spider silks.[10,11] Additionally, an optional spacer domain is incorporated between the repeat sequences of the minor ampullate and flagelliform spidroin (MiSp and FlSp, respectively) repetitive regions.[12,13] In the silk gland, the spidroins are stored at a concentration of up to 500 mg $mL^{-1}$, constituting a native spinning dope that passes through the spider's silk duct, where it undergoes a series of structural transformations leading to the formation of a solid fiber. This process involves the alignment of the protein chains,[14] their interconnection through the dimerization of the NT,[15–18] and the formation of $\beta$-sheet rich crystalline regions, potentially triggered by the CT.[19] These transformations are driven by a combination of mechanical and chemical factors, including shear forces, changes in pH, ion composition, and dehydration.[14,20,21] Prior to the extrusion of silk, glycoprotein and lipid layers are likely added to the protein fiber as protective coatings.[7,22,23]

The fundamental understanding gained about spider silk composition, its hierarchical organization, and natural spinning mechanisms has sparked the development of new technologies aimed at producing synthetic spider silk using a biomimetic approach.[24] These methodologies rely on the heterologous expression of recombinant miniature spidroins containing multiple repeat sequences along with the terminal domains.[25–27] Following purification, the mini-spidroins are subjected to chemical and physical treatments that simulate the conditions in the spider silk duct, resulting in the production of artificial fibers in a biomimetic way.[28,29] Some approaches involve subjecting the obtained (as-spun) fibers to further post-spin stretching in aqueous alcohols to enhance their mechanical properties.[25,30] Altogether, these techniques yield synthetic spider silk with a toughness modulus comparable to or slightly exceeding that of natural dragline silks.[25,31]

The mechanical properties of both natural and synthetic spider silks exhibit high variability, which can be attributed to the effects of spinning conditions[32] (e.g., spinning speed) and the humidity experienced before and during the property measurement.[33–35] Lack of humidity can make spider silk brittle, diminishing its ability to withstand stress and deformation. Artificial silks lacking a protective glycoprotein and lipid coating may be even more susceptible to the deterioration of fiber mechanical properties when they either dry out[28] or absorb excessive water.[36] This poses a threat to the long-term persistence of mechanical properties and durability of synthetic spider silk fibers.

Bioconjugation is a synthetic tool that enables modification of the 2D and 3D structure of proteins ultimately leading to tunable biomaterials. Bioconjugation of proteins enables improving their pharmacokinetics, solubility, physical and chemical stability, and immune activation. It is often accomplished by chemical modification of the parent proteins with carbodiimide or activated ester chemistry but more recently considerable progress has been made also in the click chemistry approach as well as enzyme-mediated processes.[37] To date, polyethylene glycol (PEG)-ylation has proven to be the most successful protein conjugation strategy resulting in more than 20 marketed PEG–protein conjugates, and more being on the way.[38]

The pioneering studies on the bioconjugation of spider silk proteins have been reported by the Scheibel group. For example, the surface of recombinant spider silk film was first modified using the EDC/NHS technique followed by an alkyne click reaction with the newly introduced azido group.[39] The Scheibel group also disclosed a successful expression of a recombinant protein possessing 14 cysteine fragments at N-terminus ultimately enabling bioconjugation of the cysteine thiol groups via thiol–ene click chemistry.[40] More recently Thomas and coworkers showed that by expression in an *E. coli* methionine auxotroph, the L-azidohomoalanine can be introduced residue-specifically in the mini-spidroin protein.[41] The azidogroup can in turn be further employed as a partner in subsequent click reactions. Interestingly, some other synthetic polymers like polyacrylic acid crosslinked with vinyl-functionalized silica nanoparticles have been used to prepare artificial spider silks exhibiting dragline silk-like mechanical properties by mimicking the hierarchical structure of the spider silk, including sheath-core, spiral alignment, and cross-linking.[42–44] These examples highlight the potential of spidroin–synthetic polymer composites for obtaining fibers with extraordinary mechanical properties.

Here we describe synthetic spider silk—multiarm PEG bioconjugates that enable spidroin crosslinking and chemical functionalization while retaining a biomimetic spinning approach. The PEG is introduced as a biocompatible, hydrophilic, and nontoxic polymer that does not induce an immune response[45] and at the same time may serve as a substitute for the glycoprotein and lipid coating to limit the effects of fluctuating humidity on the synthetic spider silk fibers.

## 2. Results and Discussion

### 2.1. Construct Design and Expression

To achieve biomimetic spinning of artificial spider silk, it is necessary for the recombinant mini-spidroins to exhibit high solubility and pH responsiveness. Moreover, the spinning system should accurately replicate the conditions present in the spider silk gland, including the pH gradient.[26] Taking this into account, we designed nine mini-spidroins for expression in *E. coli* comprising the NT either from *N. clavipes* flagelliform spidroin (FlSp) or *E. australis* major ampullate (dragline) spidroin 1 (MaSp1), both of which are extremely soluble and capable of dimerizing upon pH reduction to about 5.5.[8,15,17] The Rep sequences were taken from three spidroins, *E. australis* MaSp1, *N. clavipes* FlSp, and *A. argentata* tubuliform spidroin 1 (TuSp1), and incorporated one to six repeats. The CT, which forms a dimer in native spidroins, was replaced with a cysteine suitable for maleimide-thiol chemistry (**Figure 1A**). This was done with the idea that a shorter construct could result in increased protein expression yield, and bioconjugation of the cysteine to multiarm PEG would ensure the formation of dimers to octamers. Complete sequences of the designed constructs can be found in Table S1 (Supporting Information).

**Table 1** provides a summary of the expression levels, solubility after cell lysis, and protein yields of the designed mini-spidroins. Constructs with NT from *N. clavipes* FlSp generally gave higher

 

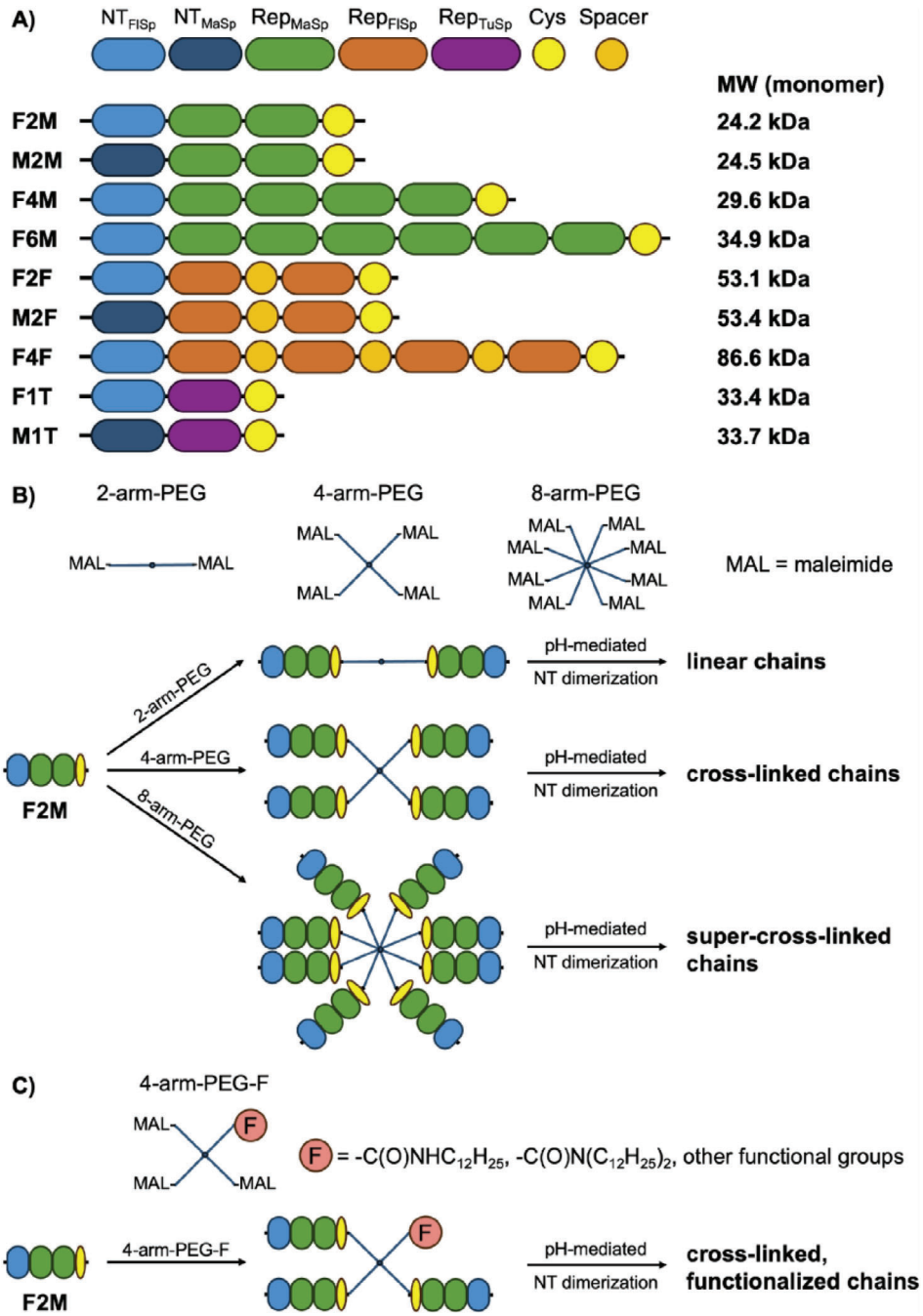


**Figure 1.** A) Domain architecture and molecular weight (MW) of the produced recombinant mini-spidroins. The sequences of the individual domains are derived from *N. clavipes* flagelliform spidroin (FlSp), *E. australis* major ampullate spidroin 1 (MaSp1), and *A. argentata* tubuliform spidroin 1 (TuSp1) (see Table S1, Supporting Information, for full sequences). The mini-spidroins are named based on the origin of the NT and the number and origin of the repetitive sequences (M for MaSp1, F for FlSp, T for TuSp1). B) Strategy for obtaining spidroin–PEG bioconjugate fibers by mini-spidroin bioconjugation with 2- to 8-arm PEG and subsequent pH-mediated polymerization. The approach is illustrated with the F2M mini-spidroin as an example. C) Strategy for obtaining chemically functionalized spidroin–PEG bioconjugate fibers by mini-spidroin bioconjugation with 2- to 8-arm PEG bearing a functional group (F) on one arm and subsequent pH-mediated polymerization. The approach is illustrated with the F2M mini-spidroin and 4-arm-PEG-F as an example.

expression levels, whereas constructs with Rep from *A. argentata* TuSp1 had lower expression levels than constructs with Rep sequences from *E. australis* MaSp1 and *N. clavipes* FlSp. As expected, an increased number of repeats reduced protein expression levels.

Constructs containing the Rep from *A. argentata* TuSp1 and more than two repeat sequences from *E. australis* MaSp1 exhibited only partial solubility after cell lysis. Nevertheless, the amount of soluble protein proved sufficient for purification using immobilized metal-affinity chromatography (IMAC), resulting in

**Table 1.** Expression level, solubility after cell lysis, and protein yield of the designed proteins. The expression level and solubility after cell lysis were assessed based on the appearance of the target band on SDS-PAGE gels (Figure S1, Supporting Information) and categorized as very high (+++), intermediate (++), low (+), and not at all (0).

| Mini-spidroin construct | Expression level | Solubility after cell lysis | Protein yield after purification, mg $L^{-1}$ of culture |
|---|---|---|---|
| F2M | +++ | +++ | 116.0 |
| M2M | ++ | +++ | 34.0 |
| F4M | ++ | ++ | 50.6 |
| F6M | ++ | + | 30.1 |
| F2F | ++ | +++ | 56.0 |
| M2F | ++ | +++ | 50.1 |
| F4F | + | +++ | 8.2 |
| F1T | + | + | 13.6 |
| M1T | + | + | 5.6 |

yields ranging from 5.6 to 116 mg of pure protein per liter of culture. The F2M construct, which contains NT from *N. clavipes* FlSp and two repeats from *E. australis* MaSp1, yielded the highest amount. Additionally, F2F, F4M and M2F also presented high yields (>50 mg per liter culture), while M2M and F6M showed intermediate yields (see Figure 1A for abbreviations). Expression and purification of the F4F, F1T, and M1T constructs did not result in sufficient protein for further studies. Based on these results, the constructs F2M, F4M, and F2F were chosen as most optimal for further bioconjugation and fiber spinning experiments. The M2F and M2M constructs were deprioritized because of a lower yield in comparison to F2F and F2M, respectively. Additionally, the F6M construct was selected for evaluating the effects of an increased repeat number on fiber spinnability.

### 2.2. Bioconjugation

To enable the tuning of physical properties as well as the chemical functionalization of artificial spider silk, we envisioned a bioconjugation strategy based on the maleimide-thiol reaction. We hypothesized that bioconjugating mini-spidroins, which contain an NT, a Rep region, and a C-terminal cysteine, with 2- to 8-arm PEG could lead to the formation of soluble mini-spidroin dimers to octamers linked by PEG. These conjugates could be further polymerized and transformed into fibers through NT-mediated dimerization at low pH (Figure 1B). This process would result in cross-linked mini-spidroins, and enable easy tuning of material properties and the introduction of new functionalities by varying the bioconjugation reaction conditions such as reactants and their stoichiometry. Therefore, we studied the bioconjugation of our mini-spidroins with homo- and heterofunctional 2- to 8-arm PEG polymers.

After purification, the recombinant mini-spidroins partially existed as disulfide-linked dimers formed by the C-terminal cysteine (Figure S2, Supporting Information). For conjugation to the maleimide-functionalized PEG, the disulfides were converted to the corresponding thiols by treatment with 10 eq of TCEP[46] for 24 h at 4 °C. To prevent interference with the subsequent bioconjugation step, any unreacted excess TCEP was removed by passing the reaction mixture through an IMAC column. The obtained protein solution was then treated with maleimide-functionalized PEGs having a molecular weight of 5–10 kDa in sodium phosphate buffer at room temperature. This process furnished the desired conjugates, which were analyzed by SDS-PAGE (Table S2, Supporting Information) as they could not be ionized using MALDI-TOF MS, and gel filtration chromatography showed insufficient resolution for estimating the degree of conjugation. PEG derivatives with aliphatic chains were synthesized from bifunctionalized PEGs having one arm with succinimide and the other(s) with maleimide, which were combined with the corresponding aliphatic amine in acetonitrile. The reaction was kept for one hour to avoid the undesired aza-Michael addition, which can occur with extended reaction times.[47] Following the reaction, the desired product was precipitated using diethyl ether and dried under vacuum before being used in the bioconjugation with mini-spidroins.

The bioconjugation efficiency, calculated as the ratio between the sum of intensities of the bioconjugation products and all protein bands in SDS-PAGE gel, varied from 42 to 83% (**Table 2**). For the F2M spidroin, the bioconjugation yields ranged from 65 to 73% and were independent of the number of PEG arms. Somewhat higher product yields of 76 to 83% were obtained with aliphatic group (C12) functionalized PEGs. However, the reaction with PEGs containing two aliphatic C12 chains resulted in a reduced yield of 47% to 70% due to their limited solubility. For the F4M and F6M spidroins, which exhibited a tendency to aggregate forming a gel at higher concentrations, the bioconjugation efficiencies with 2- and 4-arm PEGs were similar, ranging from 49 to 56%. In the case of the F2F spidroin, the bioconjugation efficiency was mostly high, ranging from 67 to 77%, regardless of the number of arms on the PEG. The only exception was the reaction with 8-arm-PEG containing an aliphatic C12 chain, which gave a yield of 42%. From the 17 spidroin bioconjugates, 13 could be concentrated to at least 150 mg $mL^{-1}$ to obtain spinning dopes, whereas four (F4M and F6M with 2- and 4-arm-PEG) precipitated during the concentration (Table 2).

### 2.3. Fiber Spinning

The spinning dopes obtained from 13 F2M and F2F spidroin bioconjugates were loaded into a syringe and extruded through a fine glass needle into a low pH aqueous buffer, following the biomimetic spinning procedure described earlier.[26] The F4M and F6M spidroin–PEG bioconjugates could not be spun into fibers due to their instability and premature aggregation at high concentrations. Fibers were obtained from one F2M and five F2F spidroin bioconjugates. The F2M conjugates with 2-arm-PEG, whether including or excluding C12 alkyl chains, as well as those with 4-arm-PEG bearing a C12 chain, and 8-arm-PEG formed fragile jelly-like fibers that could not be collected on a spinning frame. Only the F2M bioconjugate with 4-arm-PEG could be retrieved, however, spinning was only possible at low reeling rates and with a reduced distance between the needle and the reeling wheel. The poor spinnability and compromised integrity of the F2M bioconjugates may be attributed to the low mass percentage of the Rep region in these constructs, leading to insufficient intermolecular interactions. The F2F spidroin conjugates with 4- and

**Table 2.** Bioconjugation yield and spinnability of the mini-spidroin bioconjugates. The bioconjugation yield was estimated from the intensities of the unconjugated protein and the sum of the bioconjugation product bands in SDS-PAGE gels. The spinnability into fibers was categorized as very high (+++), intermediate – breaking from time to time during collection (++), low – breaking soon after the start of collection (+), and not at all (0). (–) indicates not tested. (1) indicates precipitation during protein concentration before spinning.

| Mini-spidroin construct | Bioconjugated polymer | Average bioconjugation yield [%] | Spinnability into fibers |
|---|---|---|---|
| F2M | 2-arm-PEG | 68 ± 9% | 0 |
| F2M | 2-arm-PEG-C12 | 76% | 0 |
| F2M | 2-arm-PEG-2C12 | 47% | 0 |
| F2M | 4-arm-PEG | 65 ± 10% | + |
| F2M | 4-arm-PEG-C12 | 83 ± 10% | 0 |
| F2M | 4-arm-PEG-2C12 | 70% | 0 |
| F2M | 8-arm-PEG | 73 ± 4% | 0 |
| F4M | 2-arm-PEG | 49% | 1 |
| F4M | 4-arm-PEG | 52% | 1 |
| F6M | 2-arm-PEG | 56% | 1 |
| F6M | 4-arm-PEG | 53% | 1 |
| F2F | 2-arm-PEG | 76 ± 2% | +++ |
| F2F | 4-arm-PEG | 76 ± 10% | +++ |
| F2F | 4-arm-PEG-C12 | 77% | ++ |
| F2F | 4-arm-PEG-2C12 | 73% | ++ |
| F2F | 8-arm-PEG | 67 ± 12% | +++ |
| F2F | 8-arm-PEG-C12 | 42% | 0 |
| F2F | – | – | +++ |

8-arm-PEG, including those with C12 alkyl chains, demonstrated intermediate to excellent spinnability and were successfully collected on a reeling frame positioned at the end of the spinning bath (**Figure** 2B). The visual appearance of the spun F2M- and F2F-PEG bioconjugate fibers was similar although the F2M-4-arm-PEG fibers had a rougher surface (Figure 2C). The diameter of the F2M-4-arm-PEG bioconjugate fibers, as determined by light microscopy, was larger compared to the F2F–PEG fibers (Figure 2D), consistent with the fact that the F2M–PEG bioconjugate fibers were spun at a lower reeling speed and using a reduced distance between the needle and the reeling wheel.

The F2F–PEG bioconjugate fibers were further examined by scanning electron microscopy (SEM) to compare their surface morphologies (Figure 2C). All the bioconjugate fibers show micrometer-sized sphere-like particle agglomerations on the surface. The morphology of the fiber samples F2F-2-arm-PEG, F2F-4-arm-PEG-C12, and F2F-8-arm-PEG is very similar and reveals only a few inclusions on the fibers' surfaces. It is noted that a higher number of PEG arms, which may lead to a somewhat increased PEG content, increases the generation of the surface inclusions, i.e., bead defects in the spun fibers. The F2F-4-arm-PEG and F2F-4-arm-PEG-2C12 fibers contain obvious bead inclusions on their surface structure. For the sample F2F-4-arm-PEG-2C12, the number of inclusions increased drastically and completely covered the entire fibers, while the shape of the bead inclusions transformed from spherical to irregular particles after incorporation of two C12 aliphatic chains. Notably, fibers spun from the unconjugated F2F mini-spidroin show a smooth and homogeneous surface structure, which suggests that the surface structure inclusions are comprised of PEG or aliphatic chain-functionalized PEG.

### 2.4. Mechanical Properties

The mechanical properties of fibers produced from the spidroin–PEG bioconjugates were tested in their as-spun state at low relative humidity (<30%). Despite their larger diameter, the tensile strength of F2M-4-arm-PEG conjugate fibers reached 41 MPa, comparable to that of several other as-spun synthetic spidroin fibers incorporating MaSp repeats (Figure 2E, Table S3, Supporting Information). This comparison includes other mini-spidroins with 12 to 20 repeats,[25,48] as well as MaSp1 and MaSp2 analogs produced in goat milk.[30] These findings suggest that bioconjugation with 4-arm PEG can substitute for a larger number of repeats. Conjugation with PEG also had no noticeable effect on the extensibility of the fibers, as the strain at break (6%, see Figure 2F) was similarly small compared to these other synthetic MaSp-based fibers (Table S3, Supporting Information). However, replacing the CT with 4-arm PEG seems to adversely affect fiber tensile properties as the NT2RepCT mini-spidroin comprising both terminal domains showed significantly increased strength (95 MPa) and strain (87%).[27] This highlights the importance of the CT, which is thought to mediate liquid–liquid phase separation of spidroins[49] and function as a nucleation center triggering the conversion to $\beta$-sheet structures in the MaSp repetitive domain.[19]

The tensile strength of the F2F-2-arm-PEG and F2F-4-arm-PEG fibers was similar to that of the F2M-4-arm-PEG fibers, reaching 43 and 45 MPa, respectively, while F2F-8-arm-PEG fibers displayed a doubling in tensile strength to 81 MPa, which is also three to four times higher than that of other as-spun synthetic spidroin fibers incorporating FlSp repeats (Figure 2E, Table S4, Supporting Information).[50] This exceptional

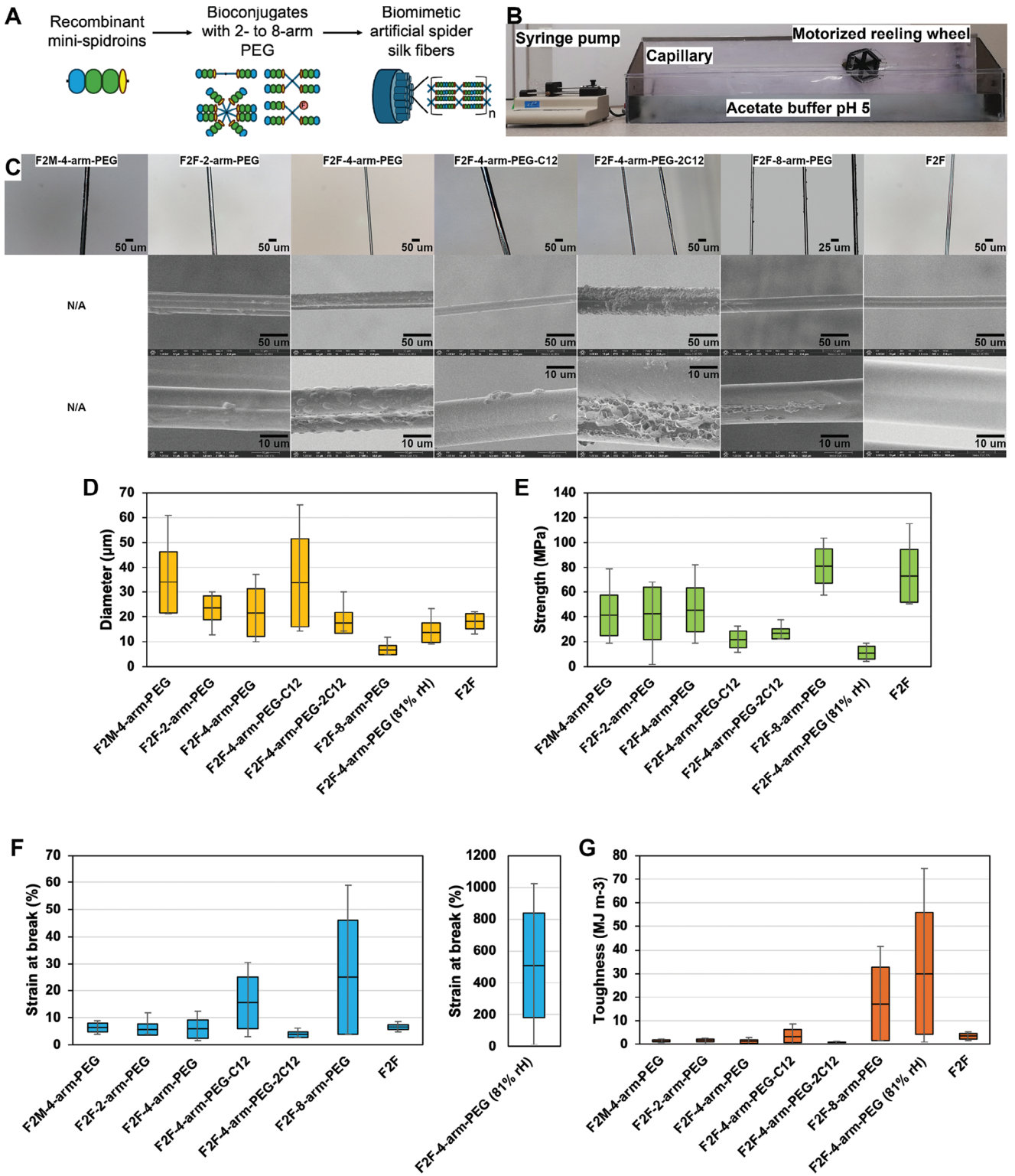


**Figure 2.** A) Schematic illustration of the fiber preparation from production of recombinant mini-spidroin to bioconjugation and biomimetic fiber spinning. B) Picture of the biomimetic spinning system. C) Light microscope images (top) and SEM micrographs (middle, bottom) of the spun fibers. D–G) Mechanical properties of the tested synthetic spider silk–PEG conjugate fibers. The boxes show ± one standard deviation from the mean value (horizontal line in the middle), and whiskers indicate the minimal and the maximal values. The properties were calculated from stress–strain curves of 8–10 individual fibers (Figure S3, Supporting Information).

performance could be partially attributed to the increased degree of bioconjugation and a significantly smaller average diameter of the fibers (6.6 µm). The strength and toughness of the F2F-8-arm-PEG fibers reach approximately 20% of that of natural flagelliform silk fibers.[11] These properties could be further improved by increasing the number of repeats in the repetitive region albeit at the expense of lower protein expression yields and by post-spin stretching as previously reported for other mini-spidroin-based artificial fibers.[51]

Although FlSp-based fibers are expected to exhibit lower tensile strength and higher extensibility than MaSp-based fibers, the strain at break was only 6% to 25% for the F2F-2-arm-PEG, F2F-4-arm-PEG and F2F-8-arm-PEG fibers, which is similar or marginally increased in comparison to F2M-4-arm-PEG fibers (Figure 2F). To assess the impact of the multiarm-PEG, we also spun fibers from the unconjugated F2F mini-spidroin. The corresponding tensile strength was 73 MPa with a strain at break of 6%. These results indicate that bioconjugation with multiarm PEG can result in elevated fiber tensile strength and extensibility albeit only at a high degree of crosslinking as achievable with 8-arm-PEG. Notably, this also leads to an increased toughness modulus of the fiber (Figure 2G).

Natural flagelliform silk contains an aqueous viscid coating, which retains high relative humidity and is responsible for its significant elasticity and supercontraction behavior.[52,53] To investigate the effect of high relative humidity on the mechanical properties of our F2F-4-arm-PEG fibers, we conducted additional testing under such conditions (81% rH, see Figure 2D–G and Table S4, Supporting Information). The results revealed a marked increase in fiber extensibility coupled with a fourfold decrease in tensile strength. The strain at break of the F2F-4-arm-PEG fibers under these conditions (507%) is, to the best of our knowledge, the highest among protein-based artificial spider silk fibers.[51] and nearly twice as large as that observed for natural flagelliform silk.[54] Similar and even higher extensibility (up to 1200%) has been observed only for synthetic polymer-based artificial spider silks.[44] From these results, it is evident that the bioconjugation of FlSp-based mini-spidroins with multiarm PEG not only preserves but also enhances the elastomeric response of these fibers in wet conditions. This effect is likely attributed to the hygroscopic properties of PEG, which enhances the absorption of water molecules and channels them to the protein chains, thereby facilitating the disruption and subsequent recreation of hydrogen bonds within the fibers. Potential applications of these super-extensible fibers include medical sutures, artificial muscles, wearable electronics, and smart textiles, where their ability to maintain flexibility and strength in humid conditions would be highly beneficial.

Besides crosslinking of spidroins, our bioconjugation approach allows the introduction of novel functional groups into the composite fibers (Figure 1C). To explore the possibility of creating a lipid coating onto the fibers, we prepared several spidroin–PEG bioconjugates bearing one or two C12 alkyl chains on one of the PEG arms as described above. Such fibers with a hydrophobic coating could be used in biodegradable outdoor textiles and medical implants, where they reduce biofouling and improve lubrication between the implant and surrounding tissues. However, only the F2F-4-arm-PEG-C12 and F2F-4-arm-PEG-2C12 bioconjugates could be successfully spun into fibers and were tested at low relative humidity conditions. The tensile strength of both F2F-4-arm-PEG-C12 and F2F-4-arm-PEG-2C12 fibers was about half that of the F2F-4-arm-PEG fibers (22 and 26 vs 45 MPa, see Figure 2E and Table S4, Supporting Information). However, the extensibility of the fibers remained relatively low (4–15%) indicating that the lipid does not protect the fiber from drying in the same way as the natural aqueous viscid coating of flagelliform silk. The reason could be the relatively low lipid mass percentage of ≈0.1%, which is about 30–50 times lower than the lipid mass ratio in natural fibers.[7] Further studies to investigate the impact of a larger lipid mass ratio as well as other chemical functionalities on the mechanical properties of artificial spider silks are warranted.

In contrast to unconjugated mini-spidroins or PEG-based materials, the dual characteristics of spidroin–PEG bioconjugates, along with their crosslinking and chemical functionalization potential, would allow for a wide range of applications and offer numerous advantages. These bioconjugates could be processed into various formats such as gels, films, sponges, and fibers, as previously reported for spidroin-based biomaterials.[55] In blends with silk fibroin, PEG was shown to reduce fibroblast adherence and scar tissue formation.[56–58] Therefore, the spidroin–PEG bioconjugates might be suitable as anti-adhesive coatings and scar-minimizing biomaterials. At the same time, the bioconjugates have enhanced mechanical properties and stability compared to PEG hydrogels. Overall, the presented data suggest that spidroin–PEG composites could be strong competitors for use in implantable materials including sutures, artificial muscles, implantable electronics, and medical implants; nevertheless further in vitro and in vivo studies are required to directly assess the application-specific properties of these biomaterials.

### 2.5. Structural Characterization

Biomimetic spinning of artificial spider silk involves the pH-dependent dimerization of the NT domain, leading to interconnected spidroins and structural transformation of the Rep domain, ensuring the formation of strong fibers. To assess the pH responsiveness of the F2F mini-spidroin and evaluate potential interactions among its NT, Rep, and Spacer domains, we conducted 2D $^{15}N$–$^{1}H$ heteronuclear single quantum coherence (HSQC) NMR measurements. **Figure 3A** shows an overlay of the HSQC NMR spectra of $^{13}C$, $^{15}N$-labeled F2F mini-spidroin at pH 7.0 and 5.5, as well as the isolated monomeric $NT_{FlSp}$ domain at pH 7.2. Considering the relatively high molecular weight of F2F (53.1 kDa), the peaks exhibit narrow linewidths, suggesting that there are no stable interactions between the individual domains of F2F and that they tumble independently. A portion of peaks in the pH 7.0 spectrum also align very closely with the spectrum of the isolated monomeric $NT_{FlSp}$ domain at pH 7.2, indicating that the NT structure is identical in the F2F mini-spidroin as it is in isolation. The remaining peaks belonging to the Rep and Spacer domains display $^{1}H$ chemical shifts in the narrow range between 7.8 and 8.2 ppm, which is characteristic of a largely unstructured conformation.

From the comparison of the F2F spectra at pH 7.0 and pH 5.5, conditions at which the isolated NT was previously found to be in a monomeric and dimeric state,[17] it is evident that the NT

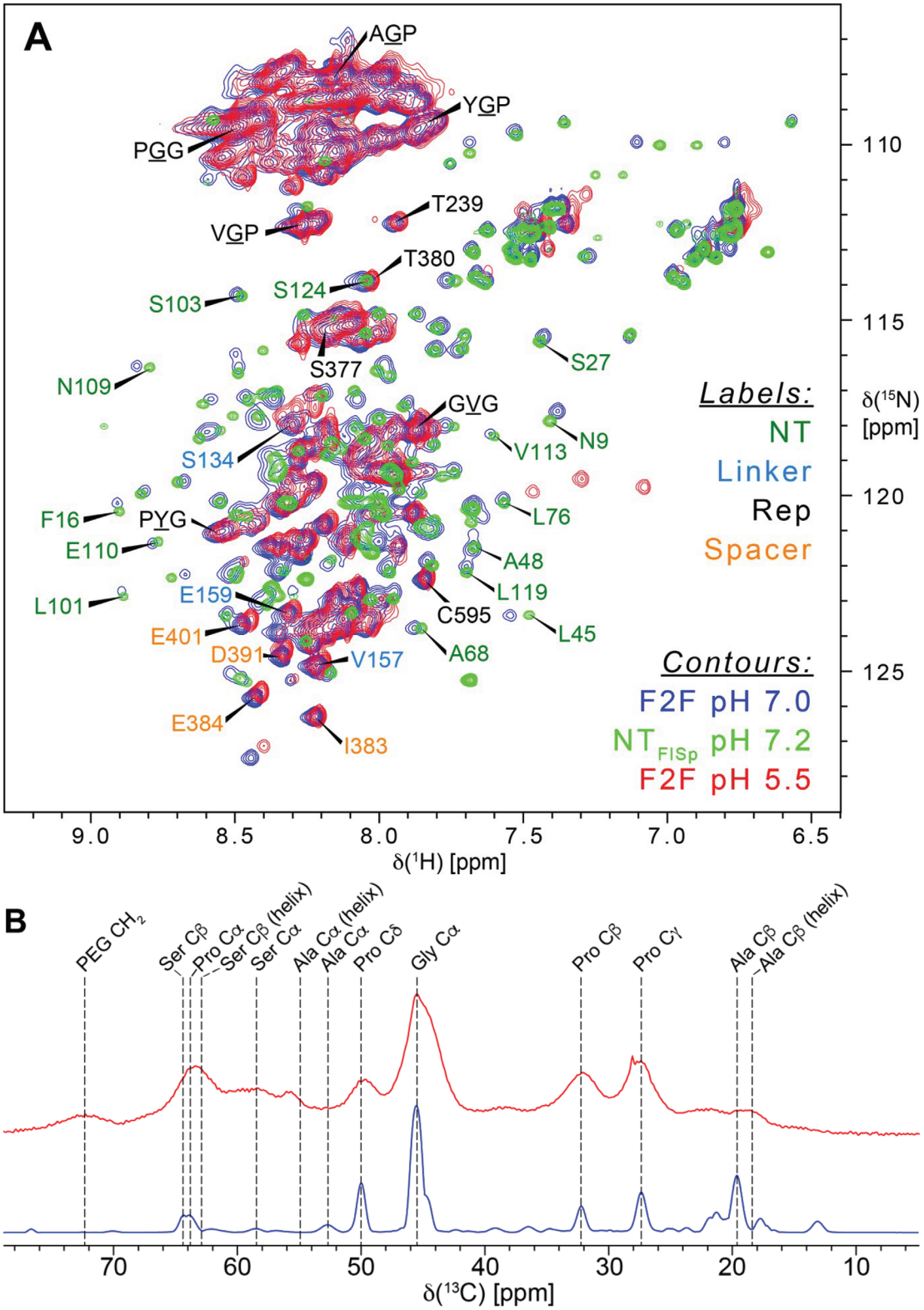


**Figure 3.** A) 600 MHz 2D $^{15}$N-$^{1}$H HSQC NMR spectrum of $^{13}$C, $^{15}$N-labeled F2F mini-spidroin at pH 7.0 (blue contours) overlaid with the spectra of isolated monomeric $NT_{FISp}$ at pH 7.2 (green contours) and F2F at pH 5.5 (red contours). Assignments of isolated peaks are indicated and colored according to location in the sequence (NT residues in dark green, linker residues between NT and Rep in light blue, Rep in black and spacer residues in orange). B) Stacked 1D $^{1}$H-$^{13}$C HSQC projection of F2F spidroin (blue) and cross-polarization (CP)-MAS NMR spectrum of F2F-4-arm-PEG fibers (red), acquired on a 600 MHz and an 800 MHz NMR spectrometer with 12 kHz MAS, respectively.

signals become broadened beyond detection at pH 5.5. An overlay with the spectrum of the isolated dimeric $NT_{FlSp}$ domain at pH 5.5 shows very few overlapping peaks (Figure S4, Supporting Information). Although the signal disappearance indicates association of the NT, this is different from our previously analyzed NT2RepCT mini-spidroin, for which the spectrum at pH 5.5 coincided with that of the isolated NT dimer.[28] This difference could be associated with the more extensive and compact Rep region in F2F compared to NT2RepCT or with interactions with other domains after dimerization. Notably, we also observed partial precipitation of the sample at pH 5.5, suggesting the formation of larger aggregates.

The spectra in Figure 3A also permit structural analysis of the Rep and Spacer domains in F2F. For this, we performed resonance assignment of the F2F backbone ($H^N$, N, C$\alpha$, C') and C$\beta$ atoms at pH 7.0 using 3D triple-resonance NMR experiments. Analysis of the $^{13}C$ chemical shift deviations from random-coil values suggested that both, the glycine-rich segments of the Rep domain and Spacer domain, are largely unstructured (Table S5 and Figure S5, Supporting Information). However, the calculation of the dihedral angles from the chemical shifts indicated that the GPG motifs adopt a type II $\beta$-turn conformation (Table S6, Supporting Information), which corresponds to their conformation in native flagelliform silk fibers.[59] Notably, no significant chemical shift perturbations were observed for the Rep and Spacer peaks between pH 7.0 and 5.5, confirming that these parts are pH unresponsive.

The $^{13}C$, $^{15}N$-labeled F2F sample was further mixed with unlabeled protein, bioconjugated to 4-arm-PEG, and spun into fibers for solid-state magic-angle spinning (MAS) NMR analysis. Figure 3B compares the $^{13}C$ spectra of F2F mini-spidroin in solution and after bioconjugation and fiber spinning. The chemical shifts of Gly and Pro residues are virtually identical between the samples, strongly suggesting that the GPG motifs form the same type II $\beta$-turn spiral in the bioconjugated fibers as in solution. However, the $^{13}C\alpha$ signals of Ala and $^{13}C\beta$ of Ser, which are mostly represented in GGX motifs, are perturbed and show no or reduced corresponding intensity in the solid-state spectrum. This could indicate that the GGX motifs are transformed into a helical conformation in the fibers, similar to native flagelliform silk,[59] as new intensity appeared at chemical shifts corresponding to a helical conformation. In summary, structural characterization of the F2F mini-spidroin and its 4-arm-PEG bioconjugate fibers reveals the pH-driven dimerization of the NT in F2F and retention of native-like structural motifs in the fibers, suggesting that these bioconjugated fibers maintain a biomimetic fiber formation mechanism.

## 3. Conclusions

We employed bioconjugation with multiarm PEG to design cross-linked and aliphatic chain-functionalized mini-spidroin PEG composites that could be spun into artificial fibers. The approach is a stepwise process, including bacterial expression of cysteine-bearing mini-spidroins, their bioconjugation with maleimide functionalized multiarm PEG, and biomimetic fiber spinning (Figure 2A). Six different types of fibers were obtained, with one (F2F-8-arm-PEG) showing improved tensile strength and increased extensibility compared to the original mini-spidroin, and another (F2F-4-arm-PEG) displaying nearly twice-increased extensibility in high humidity conditions compared to natural flagelliform silk. Furthermore, we demonstrate that the approach allows chemical functionalization of the fibers by introducing aliphatic chains in the PEG moiety. Finally, using NMR spectroscopy, we show that these bioconjugated mini-spidroins retain a biomimetic fiber formation mechanism.

## 4. Experimental Section

*Construct Design*: All the proteins that were expressed consisted of an N-terminal 6xHis-tag, a Tobacco etch virus (TEV) cleavage site, an NT from *Euprosthenops australis* MaSp1 or *Nephila clavipes* FlSp and a C-terminal cysteine. A repetitive segment incorporating one to two repeat sequences from *E. australis* MaSp1, *N. clavipes* FlSp or *Argiope argentata* TuSp1 was introduced between the NT and the C-terminal cysteine. Amino acid sequences corresponding to the designed mini-spidroins were translated into gene sequences, which were then optimized for codon usage in E. coli, and ordered from BioCat GmbH (see Table S1, Supporting Information, for full sequences). Additionally, the NotI restriction site was inserted before the C-terminal cysteine to allow for repeated multiplication of the repetitive sequences within the plasmids (Figure S6, Supporting Information).

*Protein Expression and Purification*: The constructs were used for heat shock transformation of *E. coli* BL21 (DE3) cells. A single colony was used to inoculate 50 mL of LB (containing 50 µg $mL^{-1}$ kanamycin) and grown at 30 °C overnight. The following day, the culture was diluted at 1:100 (v/v) into fresh LB medium and grown at 37 °C and 180 rpm to an $OD_{600}$ of 0.6. Protein overexpression was induced by the addition of isopropyl $\beta$-D-1-thiogalactopyranoside (IPTG) to a final concentration of 0.05 mM and the cultures were further incubated overnight at 25 °C. For F6M, a similar protocol was used, except that the protein overexpression was induced for 4 h at 20 °C.

The cells were harvested by centrifugation at 7000 *g* for 10 min and stored at −20 °C.

Cells were resuspended in the immobilized metal-affinity chromatography (IMAC) loading buffer ($20 \times 10^{-3}$ M Tris-HCl, $300 \times 10^{-3}$ M NaCl, $15 \times 10^{-3}$ M imidazole, pH 8.0) and lysed at 20 kPsi using a high-pressure cell disrupter (CF1 Cell Disruptor, Constant Systems Limited). Following centrifugation at 20 000 *g* for 40 min, the supernatant was loaded at flow rate of 1 mL $min^{-1}$ on a 20 mL HisTrap HP column (Cytiva). The column was washed with 5 column volumes of loading buffer, after which the bound proteins were eluted with $500 \times 10^{-3}$ M imidazole, $20 \times 10^{-3}$ M Tris-HCl, $300 \times 10^{-3}$ M NaCl, pH 8.0. The eluted protein fractions were analyzed by SDS-PAGE. The target protein-containing fractions were pooled, dialyzed against $20 \times 10^{-3}$ M sodium phosphate, $300 \times 10^{-3}$ M NaCl, pH 7.2, and concentrated to $0.6 \times 10^{-3}$ M for use in bioconjugation reactions.

*General Procedure A for PEG Functionalization with the Alkyl Chain*: The corresponding polymer was dissolved in dry MeCN and alkyl-amine was added (1.2 eq). After 1 h the solution was evaporated at RT and dissolved in DCM. Then the product was precipitated from diethyl ether and dried.

*2-Arm-PEG-MAL-C12*: The compound was obtained as a white solid (22 mg, 44% yield) from MAL-PEG-SCM (50 mg, 0.005 mmol, 1 eq), dodecylamine (0.97 mg, 0.0052 mmol, 1.05 eq) following general procedure A.

1H-NMR (400 MHz, CDCl3, Figure S7, Supporting Information) $\delta$: 6.70 (s, 2H), 3.88–3.37 (m, 329H), 2.51 (t, $J$ = 7.2 Hz, 2H), 1.33–1.19 (m, 19H), 0.89–0.83 (m, 4H).

*2-Arm-PEG-MAL-2C12*: The compound was obtained as a white solid (28 mg, 56% yield) from MAL-PEG-SCM (50 mg, 0.005 mmol, 1 eq), dodecylamine (1.94 mg, 0.0052 mmol, 1.05 eq) following general procedure A.

1H-NMR (400 MHz, CD3CN, Figure S8, Supporting Information) $\delta$: 6.77 (s, 2H), 4.13–2.98 (m, 2320 H), 2.39 (t, $J$ = 7.0 Hz, 2H), 1.60–1.42(m, 6H), 1.35–1.13 (m, 38 H), 0.84 (t, $J$ = 6.7 Hz, 6H).

*4-Arm-PEG-MAL-C12*: The compound was obtained as a white solid (30 mg, 60% yield) from (MAL)3-PEG-SCM (50 mg, 0.005 mmol, 1 eq), dodecylamine (0.97 mg, 0.0052 mmol, 1.05 eq) following general procedure A.

1H-NMR (400 MHz, CDCl3, Figure S9, Supporting Information) $\delta$: 6.63 (s, 6H), 4.05–3.16 (m, 960z H), 2.45 (t, $J$ = 7.2 Hz, 6H), 1.25–1.16 (m, 22H), 0.81 (t, $J$ = 6.9 Hz, 3H).

*8-Arm-PEG-MAL-C12*: The compound was obtained as a white solid (29 mg, 58% yield) from (MAL)7-PEG-SCM (50 mg, 0.005 mmol, 1 eq), dodecylamine (0.97 mg, 0.0052 mmol, 1.05 eq) following general procedure A.

1H-NMR (400 MHz, CDCl3, Figure S10, Supporting Information) $\delta$: 6.66 (s, 7H), 4.02–3.29 (m, 632H), 2.46 (t, $J$ = 7.2 Hz, 7H), 1.32–1.21 (m, 22H), 0.83 (t, $J$ = 6.8 Hz, 3H).

*General Reduction and Conjugation Procedure B*: To a $0.6 \times 10^{-3}$ M solution of spidroin in phosphate buffer ($20 \times 10^{-3}$ M, pH = 7.2) TCEP solution ($50 \times 10^{-3}$ M, 10 eq) in phosphate buffer ($20 \times 10^{-3}$ M, pH = 7.2) was added. The mixture was quickly vortexed and left at 4 °C for 24 h. After that reduced protein was purified from unreacted TCEP by nickel affinity chromatography, and immediately added to the corresponding multiarm PEG solution in phosphate buffer ($20 \times 10^{-3}$ M, pH = 7.2), and after approximately 1 h was analyzed by SDS-PAGE gel. The multiarm PEG was added at a ratio of 1.1/$n$ with respect to the reduced protein, where $n$ equals the number of arms. This corresponds to an excess of 0.1 equivalents of PEG, assuming complete reaction with all the arms (i.e., all the arms conjugated with protein). However, products with incompletely reacted PEG arms were always detected, which contributed to the depletion of PEG molecules more than products with fully reacted arms. Also, unreacted protein was measured by SDS-PAGE for all the bioconjugation reactions. Therefore, we assume that there was no unreacted PEG left over.

*Biomimetic Fiber Spinning*: Fiber spinning was performed similarly as previously described.[26] The bioconjugated mini-spidroins were concentrated in $20 \times 10^{-3}$ M Tris pH 8 buffer to approximately 150–350 mg mL$^{-1}$ or until high viscosity prevented further concentration. The mini-spidroin bioconjugates were extruded from a glass syringe (0.15 mL) having a capillary needle tip with a diameter from 40 to 60 µm into a coagulation bath containing $500 \times 10^{-3}$ M sodium acetate, $200 \times 10^{-3}$ M NaCl pH 5 buffer. The extrusion was done using a Cole Parmer 789100C syringe pump at a flow speed of 17 µL min$^{-1}$. The generated bioconjugated F2F fibers were pulled through the coagulation buffer and subsequently collected on a rotating collection frame positioned 60 cm away from the spinning needle. The rotor spun at a speed of 67 cm s$^{-1}$. For F2M fibers, owing to their increased fragility, the rotor was placed at a shorter distance of 5 cm and spun at a speed of 25 cm s$^{-1}$.

*Scanning Electron Microscopy (SEM)*: The morphology of the fibers was visualized using a Verios 5 XHR SEM scanning electron microscope (Thermo Fisher Scientific Inc.) using several magnifications.

*Tensile Testing*: The fibers were placed on a paper frame with a 1 cm × 1 cm square window and secured with double-sided tape. Then, the diameter of each fiber was measured three times with light microscopy at three arbitrary positions, yielding a total number of nine measurements. The average diameter was used to calculate the cross-sectional area assuming a round cross-section. The paper frame holding a fiber was mounted using grips in an Instron 5943 equipped with a 5 N load cell. After cutting the sides of the paper frame with scissors, the tensile test was performed using a displacement speed of 6 mm min$^{-1}$. All measurements were performed at 22 °C and at a RH of <30% unless noted otherwise. For each fiber type, 10 fibers were tensile tested, unless noted otherwise.

*NMR Spectroscopy*: Solution NMR experiments were performed at 298 K on a 600 MHz Bruker Avance Neo spectrometer equipped with a QCI-F quadruple-resonance cryoprobe. Variable pH spectra were recorded on a uniformly $^{13}$C, $^{15}$N-labeled F2F sample dissolved in $20 \times 10^{-3}$ M sodium phosphate with $300 \times 10^{-3}$ M NaCl, pH 7.0 or $20 \times 10^{-3}$ M sodium acetate with $20 \times 10^{-3}$ M NaCl, pH 5.5, containing also 0.03% (w/v) $NaN_3$, 5% $D_2O$ (v/v). Assignment of the Rep and Spacer domains was performed at pH 7.0. The following 2D and 3D spectra were recorded: $^{15}$N-$^{1}$H-HSQC, HNCA, HNCO, HN(CA)CO, HNCACB, CBCA(CO)NH, HN(CA)NNH, HN(CA)N, $^{13}$C-$^{1}$H-HSQC.

Solid-state MAS NMR spectra were acquired on an 800 MHz Bruker Avance III HD spectrometer with a HCN MAS 3.2 mm Bruker E-free probe, operating at 12 kHz MAS rate and 268 K temperature. The 1D $^{1}$H-$^{13}$C CP spectrum was acquired with a recycle delay of 3 s and 16384 scans. The 1D $^{1}$H-$^{13}$C INEPT spectrum was acquired with a recycle delay of 3 s and 1024 scans, but contained no signals. The $^{13}$C chemical shifts were referenced externally relative to adamantane $CH_2$ moiety at 38.48 ppm. For comparison with the solution $^{13}$C NMR spectrum, the calibration of the solid-state NMR spectrum was corrected for a calibration offset of −2.01 ppm due to the different reference standards (adamantane and DSS, respectively).[60] All spectra were processed and analyzed using Bruker TopSpin 3.6.1. program.

*Statistical Analysis*: Fiber tensile testing data were analyzed in MS Excel to calculate the mean values and standard deviations for presentation in Figure 2. The sample size for each statistical analysis was 10, except for F2F-4-arm-PEG-C12 fibers, which was 8.

## Supporting Information

Supporting Information is available from the Wiley Online Library or from the author.

## Acknowledgements

V.R. and J.F. contributed equally to this work. The authors acknowledge funding from the Latvian Council of Science grant no. lzp-2023/1-0308 and Latvian Institute of Organic Synthesis internal grant IG-2023-10. The authors acknowledge the access to the infrastructure and expertise of the BBCE—Baltic Biomaterials Centre of Excellence (European Union's Horizon 2020 research and innovation programme under the grant agreement No. 857287).

## Conflict of Interest

We declare the following conflict of interest: Dr. Kristaps Jaudzems and Dr. Gints Smits consult for PrintyMed Ltd., which is commercializing part of the research described in this manuscript. The terms of this arrangement have been approved by the Latvian Institute of Organic Synthesis in accordance with its policy on objectivity in research.

## Data Availability Statement

The data that support the findings of this study are available from the corresponding author upon reasonable request.

## Keywords

bioconjugation, biomaterials, silk coating, spider silk

Received: June 1, 2024
Revised: July 3, 2024
Published online: July 23, 2024

[1] M. Heim, D. Keerl, T. Scheibel, *Angew. Chem., Int. Ed.* **2009**, *48*, 3584.
[2] K. Arakawa, N. Kono, A. D. Malay, A. Tateishi, N. Ifuku, H. Masunaga, R. Sato, K. Tsuchiya, R. Ohtoshi, D. Pedrazzoli, A. Shinohara, Y. Ito, H. Nakamura, A. Tanikawa, Y. Suzuki, T. Ichikawa, S. Fujita, M. Fujiwara, M. Tomita, S. J. Blamires, J.-A. Chuah, H. Craig, C. P. Foong, G. Greco, J. Guan, C. Holland, D. L. Kaplan, K. Sudesh, B. B. Mandal, Y. Norma-Rashid, et al., *Sci. Adv.* **2022**, *8*, eabo6043.

[3] C. Radtke, C. Allmeling, K.-H. Waldmann, K. Reimers, K. Thies, H. C. Schenk, A. Hillmer, M. Guggenheim, G. Brandes, P. M. Vogt, *PLoS One* **2011**, *6*, 16990.
[4] S. Salehi, K. Koeck, T. Scheibel, *Molecules* **2020**, *25*, 737.
[5] B. Bakhshandeh, S. S. Nateghi, M. M. Gazani, Z. Dehghani, F. Mohammadzadeh, *Int. J. Biol. Macromol.* **2021**, *192*, 258.
[6] J. A. Kluge, O. Rabotyagova, G. G. Leisk, D. L. Kaplan, *Trends Biotechnol.* **2008**, *26*, 244.
[7] A. Sponner, W. Vater, S. Monajembashi, E. Unger, F. Grosse, K. Weisshart, *PLoS One* **2007**, *2*, e998.
[8] G. Askarieh, M. Hedhammar, K. Nordling, A. Saenz, C. Casals, A. Rising, J. Johansson, S. D. Knight, *Nature* **2010**, *465*, 236.
[9] F. Hagn, L. Eisoldt, J. G. Hardy, C. Vendrely, M. Coles, T. Scheibel, H. Kessler, *Nature* **2010**, *465*, 239.
[10] N. A. Ayoub, J. E. Garb, R. M. Tinghitella, M. A. Collin, C. Y. Hayashi, *PLoS One* **2007**, *2*, e514.
[11] J. M. Gosline, P. A. Guerette, C. S. Ortlepp, K. N. Savage, *J. Exp. Biol.* **1999**, *202*, 3295.
[12] G. Chen, X. Liu, Y. Zhang, S. Lin, Z. Yang, J. Johansson, A. Rising, Q. Meng, *PLoS One* **2012**, *7*, 52293.
[13] X. Qi, H. Wang, K. Wang, Y. Wang, A. Leppert, I. Iashchishyn, X. Zhong, Y. Zhou, R. Liu, A. Rising, M. Landreh, J. Johansson, G. Chen, *Adv. Funct. Mater.* **2024**, *34*, 2315409.
[14] F. Vollrath, D. P. Knight, *Nature* **2001**, *410*, 541.
[15] N. Kronqvist, M. Otikovs, V. Chmyrov, G. Chen, M. Andersson, K. Nordling, M. Landreh, M. Sarr, H. Jörnvall, S. Wennmalm, J. Widengren, Q. Meng, A. Rising, D. Otzen, S. D. Knight, K. Jaudzems, J. Johansson, *Nat. Commun.* **2014**, *5*, 3254.
[16] M. Otikovs, G. Chen, K. Nordling, M. Landreh, Q. Meng, H. Jörnvall, N. Kronqvist, A. Rising, J. Johansson, K. Jaudzems, *ChemBioChem* **2015**, *16*, 1720.
[17] M. Sarr, K. Kitoka, K.-A. Walsh-White, M. Kaldmäe, R. Metlāns, K. Tārs, A. Mantese, D. Shah, M. Landreh, A. Rising, J. Johansson, K. Jaudzems, N. Kronqvist, *J. Biol. Chem.* **2022**, *298*, 101913.
[18] M. Šede, J. Fridmanis, M. Otikovs, J. Johansson, A. Rising, N. Kronqvist, K. Jaudzems, *Front. Mol. Biosci.* **2022**, *9*, 936887.
[19] M. Andersson, G. Chen, M. Otikovs, M. Landreh, K. Nordling, N. Kronqvist, P. Westermark, H. Jörnvall, S. Knight, Y. Ridderstråle, L. Holm, Q. Meng, K. Jaudzems, M. Chesler, J. Johansson, *PLoS Biol.* **2014**, *12*, 1001921.
[20] D. Knight, F. Vollrath, *Naturwissenschaften* **2001**, *88*, 179.
[21] C. Dicko, F. Vollrath, J. M. Kenney, *Biomacromolecules* **2004**, *5*, 704.
[22] F. Vollrath, E. K. Tillinghast, *Naturwissenschaften* **1991**, *78*, 557.
[23] H. C. Salles, E. C. F. R. Volsi, M. R. Marques, B. M. Souza dos, L. D. Santos, C. F. Tormena, M. A. Mendes, M. S. Palma, *Chem. Biodiversity* **2006**, *3*, 727.
[24] A. Rising, J. Johansson, *Nat. Chem. Biol.* **2015**, *11*, 309.
[25] A. Heidebrecht, L. Eisoldt, J. Diehl, A. Schmidt, M. Geffers, G. Lang, T. Scheibel, *Adv. Mater.* **2015**, *27*, 2189.
[26] M. Andersson, Q. Jia, A. Abella, X.-Y. Lee, M. Landreh, P. Purhonen, H. Hebert, M. Tenje, C. V. Robinson, Q. Meng, G. R. Plaza, J. Johansson, A. Rising, *Nat. Chem. Biol.* **2017**, *13*, 262.
[27] B. Schmuck, G. Greco, A. Barth, N. M. Pugno, J. Johansson, A. Rising, *Mater. Today* **2021**, *50*, 16.
[28] M. Otikovs, M. Andersson, Q. Jia, K. Nordling, Q. Meng, L. B. Andreas, G. Pintacuda, J. Johansson, A. Rising, K. Jaudzems, *Angew. Chem., Int. Ed. Engl.* **2017**, *56*, 12571.
[29] N. Gonska, P. A. López, P. Lozano-Picazo, M. Thorpe, G. V. Guinea, J. Johansson, A. Barth, J. Pérez-Rigueiro, A. Rising, *Biomacromolecules* **2020**, *21*, 2116.
[30] C. G. Copeland, B. E. Bell, C. D. Christensen, R. V. Lewis, *ACS Biomater. Sci. Eng.* **2015**, *1*, 577.
[31] T. Arndt, G. Greco, B. Schmuck, J. Bunz, O. Shilkova, J. Francis, N. M. Pugno, K. Jaudzems, A. Barth, J. Johansson, A. Rising, *Adv. Funct. Mater.* **2022**, *32*, 2200986.
[32] B. Schmuck, G. Greco, F. G. Bäcklund, N. M. Pugno, J. Johansson, A. Rising, *Commun. Mater.* **2022**, *3*, 83.
[33] T. Vehoff, A. Glišović, H. Schollmeyer, A. Zippelius, T. Salditt, *Biophys. J.* **2007**, *93*, 4425.
[34] K. Yazawa, A. D. Malay, H. Masunaga, Y. Norma-Rashid, K. Numata, *Commun. Mater.* **2020**, *1*, 10.
[35] G. Greco, H. Mirbaha, B. Schmuck, A. Rising, N. M. Pugno, *Sci. Rep.* **2022**, *12*, 3507.
[36] G. Greco, T. Arndt, B. Schmuck, J. Francis, F. G. Bäcklund, O. Shilkova, A. Barth, N. Gonska, G. Seisenbaeva, V. Kessler, J. Johansson, N. M. Pugno, A. Rising, *Commun. Mater.* **2021**, *2*, 43.
[37] S. A. L. Matthew, F. P. Seib, *ACS Biomater. Sci. Eng.* **2024**, *10*, 12.
[38] *Polymer-Protein Conjugates: From PEGylation and Beyond*, (Eds: G. Pasut, S. Zalipsky), Elsevier, Amsterdam **2020**.
[39] J. G. Hardy, A. Pfaff, A. Leal-Egaña, A. H. E. Müller, T. R. Scheibel, *Macromol. Biosci.* **2014**, *14*, 936.
[40] K. Spieß, S. Wohlrab, T. Scheibel, *Soft Matter* **2010**, *6*, 4168.
[41] D. Harvey, P. Bardelang, S. L. Goodacre, A. Cockayne, N. R. Thomas, *Adv. Mater.* **2017**, *29*, 1604245.
[42] Y. Dou, Z.-P. Wang, W. He, T. Jia, Z. Liu, P. Sun, K. Wen, E. Gao, X. Zhou, X. Hu, J. Li, S. Fang, D. Qian, Z. Liu, *Nat. Commun.* **2019**, *10*, 5293.
[43] W. He, D. Qian, Y. Wang, G. Zhang, Y. Cheng, X. Hu, K. Wen, M. Wang, Z. Liu, X. Zhou, M. Zhu, *Adv. Mater.* **2022**, *34*, 2201843.
[44] A. Q. Khan, M. Shafiq, J. Li, K. Yu, Z. Liu, X. Zhou, M. Zhu, *SmartMat* **2023**, *4*, e1189.
[45] J. S. Suk, Q. Xu, N. Kim, J. Hanes, L. M. Ensign, *Adv. Drug Delivery Rev.* **2016**, *99*, 28.
[46] E. B. Getz, M. Xiao, T. Chakrabarty, R. Cooke, P. R. A. Selvin, *Anal. Biochem.* **1999**, *273*, 73.
[47] G. J. Noordzij, C. H. R. M. Wilsens, *Front. Chem.* **2019**, *7*, 729.
[48] F. Teulé, W. A. Furin, A. R. Cooper, J. R. Duncan, R. V. Lewis, *J. Mater. Sci.* **2007**, *42*, 8974.
[49] A. Leppert, G. Chen, D. Lama, C. Sahin, V. Railaite, O. Shilkova, T. Arndt, E. G. Marklund, D. P. Lane, A. Rising, M. Landreh, *Nano Lett.* **2023**, *23*, 5836.
[50] S. L. Adrianos, F. Teulé, M. B. Hinman, J. A. Jones, W. S. Weber, J. L. Yarger, R. V. Lewis, *Biomacromolecules* **2013**, *14*, 1751.
[51] B. Schmuck, G. Greco, T. B. Pessatti, S. Sonavane, V. Langwallner, T. Arndt, A. Rising, *Adv. Funct. Mater.* **2023**, 2305040, https://doi.org/10.1002/adfm.202305040.
[52] F. Vollrath, D. T. Edmonds, *Nature* **1989**, *340*, 305.
[53] G. V. Guinea, M. Cerdeira, G. R. Plaza, M. Elices, J. Pérez-Rigueiro, *Biomacromolecules* **2010**, *11*, 1174.
[54] T. A. Blackledge, A. P. Summers, C. Y. Hayashi, *Zoology* **2005**, *108*, 41.
[55] M. Widhe, H. Bysell, S. Nystedt, I. Schenning, M. Malmsten, J. Johansson, A. Rising, M. Hedhammar, *Biomaterials* **2010**, *31*, 9575.
[56] C. Acharya, T. V. Kumary, S. K. Ghosh, S. C. Kundu, *J. Biomater. Sci., Polym. Ed.* **2009**, *20*, 543.
[57] Y. Wang, M. Liang, Z. Zheng, L. Shi, B. Su, J. Liu, D. L. Kaplan, B. Zhang, X. Wang, *Adv. Healthcare Mater.* **2015**, *4*, 2120.
[58] J. C. Bragg, H. Kweon, Y. Jo, K. G. Lee, C. Lin, *J. Appl. Polym. Sci.* **2016**, *133*, app43075.
[59] M. Humenik, T. Scheibel, A. Smith, in *Progress in Molecular Biology and Translational Science*, Vol. *103* (Ed: S. Howorka), Elsevier, Amsterdam **2011**, pp. 131–185.
[60] C. R. Morcombe, K. W. Zilm, *J. Magn. Reson.* **2003**, *162*, 479.